

Extended phase space thermodynamics for dyonic black holes with a power Maxwell field

Feiyu Yao^{*} and Jun Tao[†]

Center for Theoretical Physics, College of Physics, Sichuan University, Chengdu 610064, China

 (Received 11 September 2020; accepted 16 May 2022; published 8 June 2022)

In this paper, we investigate the thermodynamics of dyonic black holes with the presence of power Maxwell electromagnetic field in the extended phase space, which regards the cosmological constant Λ as a thermodynamic variable. For a generic power Maxwell black hole with the electric charge and magnetic charge, the equation of state is given as the function of rescaled temperature \tilde{T} in terms of other rescaled variables \tilde{r}_+ , \tilde{q} , and \tilde{h} , where r_+ is the horizon radius, q is the electric charge, and h is the magnetic parameter. For some values of \tilde{q} and \tilde{h} , the phase structure of the black hole is uniquely determined. Moreover, the peculiarity of multiple temperature with some parameter configurations results in complex phase structures. Focusing on the power Maxwell Lagrangian with $\mathcal{L}(s) = s^2$, we obtain the corresponding phase diagrams in the \tilde{h} - \tilde{q} plane where the critical line extends to $\tilde{h} = +\infty$. Then, we analyze the black holes' phase structure and critical behavior and display phase transition curves with different \tilde{h} in the \tilde{q} - \tilde{T} plane. We also examine thermal stabilities of these black holes.

DOI: [10.1103/PhysRevD.105.124018](https://doi.org/10.1103/PhysRevD.105.124018)

I. INTRODUCTION

Black holes are intriguing concepts from the two cornerstones of modern theoretical physics: general relativity and quantum field theory. Black holes in the classical sense absorbed all matter, emitted nothing, and had neither temperature nor entropy, which were characterized by mass, angular momentum, and charge (if any) [1]. However, there is another case considering quantum field theory in curved spacetime. The relationship between black holes and thermodynamics was first indicated by Hawking's area theorem [2], which states that the area of the event horizon of a black hole can never decrease. Bekenstein subsequently noticed the similarity between this theorem and the second law of thermodynamics [3], proposing that each black hole should be assigned an entropy proportional to the area of its event horizon [4]. Analogous to the laws of thermodynamics, Bardeen *et al.* soon established the four laws of black hole mechanics [5], where the surface gravity corresponds to the temperature. Since Hawking discovered that black holes do emit radiation with a blackbody spectrum [6], the idea of black hole thermodynamics has convinced most physicists.

According to cosmological constant Λ , black holes can be classified into asymptotically de Sitter (dS) black holes ($\Lambda > 0$), asymptotically anti-de Sitter (AdS) black holes ($\Lambda < 0$), and asymptotically flat black holes ($\Lambda = 0$).

Sufficiently large asymptotically AdS (as compared to the AdS radius l) black holes, unlike asymptotically flat black holes, have positive specific heat and can be in stable equilibrium at a fixed temperature [7]. Moreover, unlike asymptotically dS black holes [8], asymptotically AdS black holes only have one horizon, and one can define a good notion of the asymptotic mass. Therefore, the research on the asymptotically AdS black holes has received great attention. Studying the phase transitions of asymptotically AdS black holes is primarily motivated by AdS/CFT correspondence [9]. Hawking and Page showed that a first-order phase transition occurs between Schwarzschild AdS black holes and thermal AdS space [7], which was later understood as a confinement/deconfinement phase transition in the context of the AdS/CFT correspondence [10]. For Reissner-Nordstrom (RN) AdS black holes, the authors of Refs. [11,12] showed that its critical behavior is similar to that of a van der Waals liquid/gas phase transition.

Soon after, the asymptotically AdS black holes were studied in the context of extended phase space thermodynamics, where the cosmological constant is interpreted as thermodynamic pressure [13,14]. In this case, the black hole mass should be understood as enthalpy instead of the internal energy; the first law was modified [15]. The P - V criticality study has been explored for various AdS black holes [16–21]. It showed that the P - V critical behaviors of AdS black holes are similar to that of a van der Waals liquid/gas system.

Nonlinear electrodynamics (NLED) is an effective model incorporating quantum corrections to Maxwell electromagnetic theory. Coupling this model to gravity,

^{*}yaofeiyu@stu.scu.edu.cn

[†]Corresponding author.
taojun@scu.edu.cn

various NLED charged black holes have been derived and discussed in a number of papers [22–31]. The thermodynamics of generic NLED black holes in the extended phase space have been considered in Refs. [32–36]. And various particular NLED black holes were also considered, e.g., Born-Infeld AdS black holes [37,38], power Maxwell invariant black holes [39–41], and nonlinear magnetic-charged dS black holes [42].

Among the various NLED theories, a straightforward generalization of Maxwell's theory leads to the so-called power Maxwell (PM) theory described by a Lagrangian density of the form $L(s) = s^p$, where s is the Maxwell invariant and p is an arbitrary rational number. It is obvious that the special value $p = 1$ corresponds to linear electrodynamics. The solutions of PM charged black holes and their interesting thermodynamics and geometric properties have been examined in Refs. [26,43–50].

In general, the Einstein equations with a matter source possessing the conformal invariance can be simplified. In the absence of the cosmological constant, a traceless energy-momentum tensor implies that the scalar curvature is zero, which restricts the possible spacetimes. A well-known example is given by the specified Bocharova-Bronnikov-Melnikov-Bekenstein (BBMB) black hole in four dimensions where the matter is described by a scalar field nonminimally coupled to gravity with the conformal coupling (and also with an electric field) [51]. In this example, the conformal character of the matter source is crucial since the solution has been derived using the machinery of conformal transformations applied to minimally coupled scalar fields. Moreover, conformal symmetry of the matter source can also be useful for gravity with a nonzero cosmological constant. In this case, the traceless character of the source imposes the spacetime to be of constant scalar curvature. However, there does not exist a no-hair theorem that rules out regular black hole solutions on and out of the event horizon. In fact, black hole solutions with a cosmological constant have been obtained given a conformally and self-interacting coupled scalar field in three dimensions [52,53] and in four dimensions [54,55].

However, Xanthopoulos and Dialynas [56] and Klimcik [57] found that the black hole solutions don't always exist for a static spherically symmetric spacetime coupled to a conformal scalar field. They have shown that in higher dimensions a scalar field conformally coupled to gravity does not exhibit black hole solutions. The RN black hole in four dimensions is the first solution with a conformally invariant matter source from the Maxwell action. However, as mentioned above, the Maxwell action of the RN solution no longer possesses the conformal symmetry [58] when it is extended to higher dimensions. A legitimate question is whether there exists an extension of the Maxwell action in arbitrary dimensions that possesses the conformal invariance, which inspires us to propose the generalized Maxwell action in arbitrary dimensions

$$I_M = - \int d^d x \sqrt{-g} s^p, \quad (1)$$

where s is the Maxwell invariant and p is an arbitrary rational number. This action enjoys the conformal invariance, which provides the exponent $p = d/4$. Note that in four dimensions the conformal action (1) reduces to the Maxwell action. It is clear that when $p = d/4$ the conformal invariance of the action is encoded by the traceless condition $T_\mu^\mu = 0$. [Consider the Lagrangian of the form $L(F)$, where $F = F_{\mu\nu} F^{\mu\nu}$; then, one can show that for this form of Lagrangian in d dimensions $T_\mu^\mu = 4(FdL/dF - d/4L)$, so $T_\mu^\mu = 0$ implies $L(F) = \text{Constant} \times F^{d/4}$.] Moreover, there also exists another conformally invariant extension of the Maxwell action in higher dimensions for which the Maxwell field is replaced by a $d/2$ form when d is even [59]. The black hole solutions of this theory are discussed in Ref. [60]. In addition, taking into account the applications of the AdS/CFT correspondence to superconductivity, it has been shown that the PM theory makes crucial effects on the condensation as well as the critical temperature of the superconductor and its energy gap [61].

A substantial gap in these studies is the absence of the dyonic solution. Bronnikov [62] derived a scheme of finding the dyonic solution in NLED coupled to GR by quadratures for an arbitrary Lagrangian function $L(s)$ and a dyonic solution for the truncated Born-Infeld theory. However, there are only few papers devoted to studies of specific cases with the dyonic solution. In this paper, we first investigate the thermodynamic behavior of generic d -dimensional dyonic PM black holes in the extended phase space in Sec. II. Then, we investigate the phase structure and critical behavior of eight-dimensional dyonic PM black holes with a power exponent 2 by studying the phase diagrams in the $q/l^{4.5}$ - $h/l^{1.5}$ plane in Sec. III. We summarize our results in Sec. IV. We will use the units $\hbar = c = 16\pi G = 1$ for simplicity.

II. DYONIC PM ADS BLACK HOLE

In this section, we derive the d -dimensional dyonic PM asymptotically AdS black hole solution in the Einstein gravity and verify the thermodynamic properties of the black hole. We first consider a d -dimensional model of gravity coupled to a PM nonlinear electromagnetic field with the action given by

$$S_{\text{Bulk}} = \int d^d x \sqrt{-g} [R - 2\Lambda + \mathcal{L}(s)], \quad (2)$$

where

$$\Lambda = - \frac{(d-1)(d-2)}{2l^2} \quad (3)$$

is the cosmological constant,

$$s = \frac{1}{4} F_{\mu\nu} F^{\mu\nu} \quad (4)$$

is the maxwell invariant, $F = dA = \partial_\mu A_\nu - \partial_\nu A_\mu$, and A_μ is the gauge potential. In our case, the Lagrangian density has the following form:

$$\mathcal{L}(s) = s^p. \quad (5)$$

Taking the variation of the action (2) with respect to $g_{\mu\nu}$ and A_μ , one can get the equations of motion, which are

$$R_{\mu\nu} - \frac{1}{2} R g_{\mu\nu} - \frac{(d-2)(d-1)}{2l^2} g_{\mu\nu} = \frac{T_{\mu\nu}}{2}, \quad (6)$$

$$\partial_\mu (\sqrt{-g} G^{\mu\nu}) = 0, \quad (7)$$

where

$$T_{\mu\nu} = g_{\mu\nu} \mathcal{L}(s) + \frac{\partial \mathcal{L}(s)}{\partial s} F_\mu{}^\rho F_{\nu\rho} \quad (8)$$

is the energy-momentum tensor and we define the auxiliary field

$$G^{\mu\nu} = \frac{\partial \mathcal{L}(s)}{\partial s} F^{\mu\nu}. \quad (9)$$

To construct a dyonic black hole solution in asymptotically AdS spacetime, we take the ansatz for the metric and the gauge potential

$$ds^2 = -f(r) dt^2 + \frac{1}{f(r)} dr^2 + r^2 d\Omega_{d-2}^2, \quad (10)$$

$$A = A_t(r) dt - h \left(\prod_{i=1}^{d-4} \sin^2 \theta_i \right) \cos \theta_{d-3} d\theta_{d-2}, \quad (11)$$

where $d\Omega_{d-2}^2$ is the metric of $(d-2)$ -sphere (only consider the case of positive constant curvature, i.e., $k=1$)

$$d\Omega_1^2 = d\theta_1^2, \quad (12)$$

$$d\Omega_{n+1}^2 = d\Omega_n^2 + \left(\prod_{i=1}^n \sin^2 \theta_i \right) d\theta_{n+1}^2. \quad (13)$$

Then, the equations of motion read

$$\begin{aligned} \frac{(d-2)}{2} r f(r)' + \frac{(d-2)(d-3)}{2} [f(r) - 1] \\ - \frac{(d-2)(d-1)r^2}{2l^2} = \frac{r^2}{2} [\mathcal{L}(s) + G^{rt} A_t'(r)], \end{aligned} \quad (14)$$

$$\partial_r (r^{d-2} G^{rt}) = 0, \quad (15)$$

$$\partial_{\theta_{d-3}} (\sin \theta_{d-3} G^{\theta_{d-3} \theta_{d-2}}) = 0. \quad (16)$$

Plugging Eq. (11) into Eq. (4) and Eq. (9) results in

$$s = \frac{A_t^2(r)}{2} - \frac{h^2}{2r^4} \quad \text{and} \quad G^{rt} = -\frac{\partial \mathcal{L}(s)}{\partial s} A_t'(r). \quad (17)$$

Equation (16) can result in $\partial_{\theta_{d-3}} h = 0$, and the remaining equations of motion can be derived from Eqs. (14) and (15). Now, $A_t'(r)$ can be determined by Eq. (15), which leads to

$$\frac{\partial \mathcal{L}(s)}{\partial s} A_t'(r) = \frac{q}{r^{d-2}}, \quad (18)$$

where q is a constant. Moreover, integrating Eq. (14), we have

$$f(r) = 1 + \frac{r^2}{l^2} - \frac{m}{r^{d-3}} - \frac{1}{(d-2)r^{d-3}} \int_r^\infty dr r^{d-2} \left[\mathcal{L} \left(\frac{A_t^2(r)}{2} - \frac{h^2}{2r^4} \right) - \frac{q}{r^{d-2}} A_t'(r) \right], \quad (19)$$

where m is a constant. Considering $L(s) = s^p$, it can be expressed analytically near the event horizon r_+ as

$$f(r) = \frac{d-3}{r_+} (r-r_+) + \frac{(d-1)r_+}{l^2} (r-r_+) - \frac{2^{-p} r_+^{2-4p} (A_{t0}^2 r_+^4 - h^2)^{p-1} (h^2 + A_{t0}^2 (2p-1) r_+^4)}{(d-2)r_+} (r-r_+) + O(r-r_+), \quad (20)$$

where $A'_{t0} \equiv A'_t(r_+)$ can be solved by Eq. (18) and we have used $f(r_+) = 0$ and Eq. (14). The Hawking temperature of the black hole is given by

$$T = \frac{f'(r_+)}{4\pi}, \quad (21)$$

so one can get

$$T = \frac{1}{4\pi r_+} \left\{ d - 3 + \frac{(d-1)r_+^2}{l^2} + \frac{1}{d-2} r_+^2 \left[\mathcal{L} \left(\frac{A_t'^2(r)}{2} - \frac{h^2}{2r^4} \right) - \frac{q}{r^{d-2}} A_t'(r_+) \right] \right\}, \quad (22)$$

which results from plugging $f(r_+) = 0$ into Eq. (14).

The electric charge is [63]

$$\begin{aligned} Q &= \int_S \bar{F} = \int \left(\prod_{i=1}^{d-2} d\theta_i \right) \bar{F} \\ &= \int \left(\prod_{i=1}^{d-2} d\theta_i \right) \sqrt{-g} \frac{q}{r^{d-2}} = \omega_{d-2} q, \end{aligned} \quad (23)$$

where

$$\bar{F} = \frac{\partial \mathcal{L}}{\partial s} (*F), \quad (24)$$

with ω_{d-2} being the volume of the unit $(d-2)$ -sphere:

$$\omega_{d-2} = \frac{2\pi^{\frac{d-1}{2}}}{\Gamma(\frac{d-1}{2})}. \quad (25)$$

Moreover, the mass can be extracted by comparison to a reference background, e.g., vacuum AdS. So, the mass can be determined by the Komar integral

$$M = \frac{d-2}{8\pi(d-3)} \int_{\partial\Sigma} dx^{d-2} \sqrt{\gamma'} (\sigma_\mu n_\nu \nabla^\mu K^\nu) - M_{\text{AdS}}, \quad (26)$$

where K^μ is the Killing vector associated with t , M_{AdS} is Komar integral associated with K^μ for the vacuum AdS space

$$M_{\text{AdS}} = \frac{d-2}{8\pi(d-3)} \int_{\partial\Sigma} dx^{d-2} \sqrt{\gamma'} \left(\frac{r}{l^2} \right), \quad (27)$$

and γ' is the induced metric of $\partial\Sigma$, which is the boundary of Σ . σ_μ is the unit normal vector of Σ , and n_μ is the unit outward-pointing normal vector. We set Σ and $\partial\Sigma$ to be a constant- t hypersurface and a $(d-2)$ -sphere at $r = \infty$.

$$M = \frac{d-2}{16\pi} \omega_{d-2} \left\{ r_+^{d-3} + \frac{r_+^{d-1}}{l^2} - \frac{1}{d-2} \int_{r_+}^{\infty} dr r^{d-2} \left[\mathcal{L} \left(\frac{A_t'^2(r)}{2} - \frac{h^2}{2r^4} \right) - A_t'(r) \frac{q}{r^{d-2}} \right] \right\}, \quad (34)$$

where we have used Eq. (33).

The free energy F can be expressed by the Euclidean action S^E [32],

$$F = M - TS, \quad (35)$$

Using

$$\sigma_\mu = (-f^{\frac{1}{2}}, 0, 0, 0, \dots), \quad (28)$$

$$n_\mu = (0, f^{-\frac{1}{2}}, 0, 0, \dots), \quad (29)$$

one can have

$$\sigma_\mu n_\nu \nabla^\mu K^\nu = \frac{1}{2} f'(r). \quad (30)$$

It is shown that for

$$d-1 < 4p < 2d-2 \quad (31)$$

one can have

$$\frac{1}{2} f'(r) = \frac{r}{l^2} + \frac{(d-3)m}{2r^{d-2}} + O(r^{2-d}) \quad (32)$$

at spatial infinity, and whether it holds or not is determined by the relationship of power exponent p and dimension d . When it holds, we have

$$M = \frac{d-2}{16\pi} \omega_{d-2} m. \quad (33)$$

In the following, we study the thermodynamics of the dyonic PM AdS black hole solution in the extended phase space, where the cosmological constant is interpreted as the thermodynamic pressure and treated as a thermodynamic variable. The mass of the black hole is no longer regarded as internal energy; it is identified with the chemical enthalpy. In terms of the horizon radius r_+ , the mass of the black hole can be rewritten as

where the entropy of the black hole is one-quarter of the horizon area

$$S = \frac{r_+^{d-2} \omega_{d-2}}{4}. \quad (36)$$

We have expressed thermodynamic quantities F , M , and S as the functions of the horizon radius r_+ , q (proportional to the electric charge Q), h (associated with magnetic charge), and the AdS radius l (the pressure $P = (d-1)(d-2)/l^2$). Now, we need to express the thermodynamic quantities in terms of T , q , h , and P by solving the equation of state for

$$r_+ = r_+(T, q, l, h). \quad (37)$$

So, we first rescale the T , which becomes

$$\tilde{T} = \frac{1}{4\pi\tilde{r}_+} \left\{ d-3 + (d-1)\tilde{r}_+^2 + \frac{\tilde{r}_+^2}{d-2} \left[\left(\frac{\tilde{A}'_t(r_+)}{2} - \frac{\tilde{h}^2}{2\tilde{r}_+^4} \right)^p - \tilde{A}'_t(r_+) \frac{\tilde{q}}{\tilde{r}_+^{d-2}} \right] \right\}, \quad (38)$$

where

$$\begin{aligned} \tilde{r}_+ &= r_+ l^{-1}, & \tilde{q} &= q l^{-\frac{1}{p}-d+4}, & \tilde{A}'_t(r_+) &= l^{\frac{1}{p}} A'_t(r_+), \\ \tilde{h} &= h l^{\frac{1}{p}-2}, & \tilde{T} &= T l. \end{aligned} \quad (39)$$

Then, $\tilde{A}'_t(r_+)$ is determined by

$$\left(p \frac{\tilde{A}'_t{}^2(r_+)}{2} - \frac{\tilde{h}^2}{2\tilde{r}_+^4} \right)^{p-1} \tilde{A}'_t(r_+) = \frac{\tilde{q}}{\tilde{r}_+^{d-2}}, \quad (40)$$

which usually cannot be solved analytically and has multiple solutions when p is large. By solving Eq. (38), \tilde{r}_+ can be expressed as a function of \tilde{T} , \tilde{q} , and \tilde{h} . With $\tilde{r}_+ = \tilde{r}_+(\tilde{T}, \tilde{q}, \tilde{h})$, one can express the thermodynamic

quantities in terms of \tilde{T} , \tilde{q} , and \tilde{h} ; e.g., the Gibbs free energy is given by

$$\tilde{F} \equiv F/l^{d-3} = \tilde{F}(\tilde{T}, \tilde{q}, \tilde{h}). \quad (41)$$

The phase structure of the black hole comes from the solutions of Eq. (38). If $\tilde{T}(\tilde{r}_+, \tilde{q}, \tilde{h})$ is a monotonic function with respect to \tilde{r}_+ for some values of \tilde{q} and \tilde{h} , there would be only one branch for the black hole. Generally, with fixed \tilde{q} and \tilde{h} , there exists a local minimum/maximum for $\tilde{T}(\tilde{r}_+, \tilde{q}, \tilde{h})$ at $\tilde{r}_+ = \tilde{r}_{+, \min}/\tilde{r}_{+, \max}$. In this case, there is more than one black hole (BH) branch, namely, small BH and large BH, around a local minimum of $\tilde{T} = \tilde{T}_{\min}$ as shown in Fig. 1(a). In the right panel of Fig. 1(a), the Gibbs free energy of these two branches is displayed, and the upper branch is a small BH while the lower one is a large BH since $\partial\tilde{F}(\tilde{T}, \tilde{q}, \tilde{h})/\partial\tilde{T} = -4\pi^6\tilde{r}_+^6$, which means that the large BH branch is thermodynamically preferred. Similarly, there are also two branches around a local maximum of \tilde{T} . In this case, the upper/lower branch is large/small BH since it has more/less negative slope, and the small BH branch is thermodynamically preferred in this case. In general, one might need to figure out how the existence of local extremums depends on values of \tilde{Q} and \tilde{h} to study the phase structure of the black hole.

Moreover, by solving Eq. (40), we can find more than one $\tilde{T}(\tilde{r}_+, \tilde{q}, \tilde{h})$ with some fixed \tilde{q} and \tilde{h} , indicating multiple sets of $\tilde{r}_{+i} = \tilde{r}_{+i}(\tilde{T}, \tilde{q}, \tilde{h})$. And every set of $\tilde{r}_{+i}(\tilde{T}, \tilde{q}, \tilde{h})$ may have multiple branches. A simple case is depicted in Fig. 1(b), which corresponds to those of Fig. 1(a).

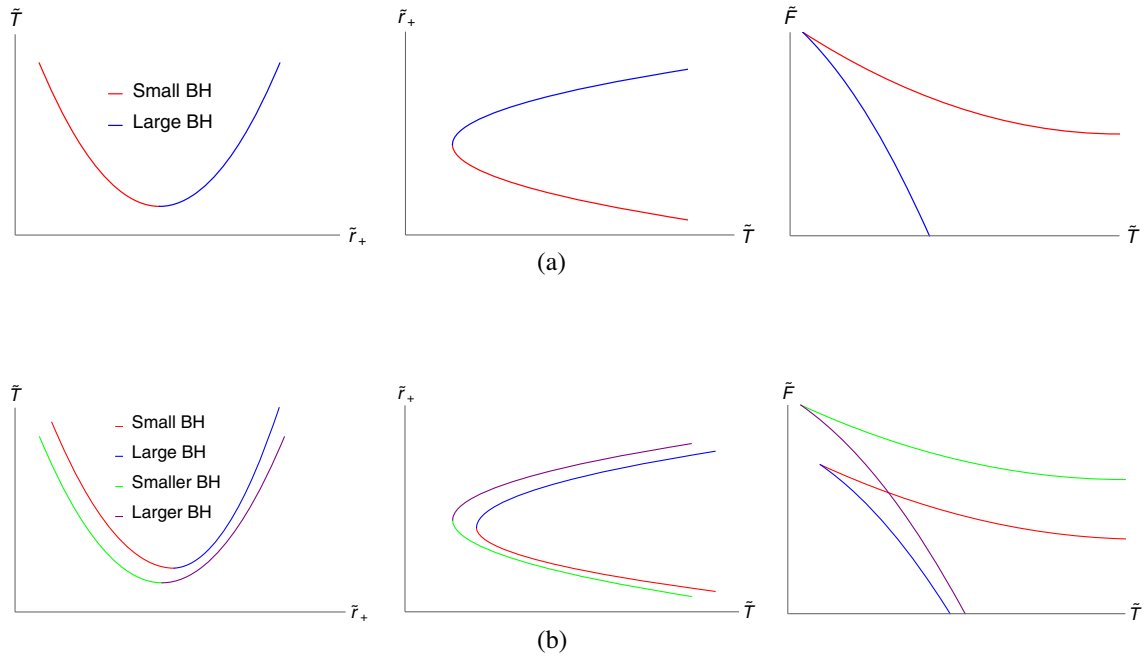


FIG. 1. Branches of black holes around local extremums of $\tilde{T} = \tilde{T}_{\min}$ and $\tilde{T} = \tilde{T}_{\max}$ with some fixed \tilde{q} and \tilde{h} . (a) Branches around a local minimum of $\tilde{T} = \tilde{T}_{\min}$. (b) Branches around a local maximum of $\tilde{T} = \tilde{T}_{\min}$ when $\tilde{T} = \tilde{T}(\tilde{r}_+, \tilde{q}, \tilde{h})$ is multivalued.

After the black hole branches are obtained, it is easy to check their thermodynamic stabilities against thermal fluctuations. The thermal stability of the branch follows from the specific heat $C > 0$. The specific heat takes the form as

$$C_{Q,h,P} = T \left(\frac{\partial S}{\partial T} \right)_{Q,h,P} = l^{d-2} (d-2) \tilde{T} \frac{\tilde{r}_+^{d-3} \omega_{d-2}}{4} \left(\frac{\partial \tilde{r}_+}{\partial \tilde{T}} \right), \quad (42)$$

and since ω_{d-2} is also positive, the sign of $\tilde{T}'(\tilde{r}_+)$ determines the thermodynamic stabilities.

III. EIGHT-DIMENSIONAL DYONIC PM ADS BLACK HOLE WITH P=2

In this section, we focus on eight-dimensional (8D) spacetime in order to satisfy the condition of conformal invariance, and the power exponent is chosen as $p = 2$. Then, the mass of the black hole satisfies

$$M = \frac{2}{5} \pi^2 \left\{ r_+^5 + \frac{r_+^7}{l^2} - \frac{1}{6} \int_{r_+}^{\infty} dr r^6 \left[\mathcal{L} \left(\frac{A_l'^2(r)}{2} - \frac{h^2}{2r^4} \right) - A_l'(r) \frac{q}{r^6} \right] \right\}, \quad (43)$$

and the electric charge

$$Q = \frac{16\pi^3}{15} q, \quad (44)$$

where we have used Eqs. (34) and (23). And Eqs. (38) and (36) become

$$\tilde{T} = \frac{1}{4\pi\tilde{r}_+} \left\{ 5 + 7\tilde{r}_+^2 + \frac{\tilde{r}_+^2}{6} \left[\left(\frac{\tilde{A}'_i{}^2(r_+)}{2} - \frac{\tilde{h}^2}{2\tilde{r}_+^4} \right)^2 - \tilde{A}'_i(r_+) \frac{\tilde{q}}{\tilde{r}_+^6} \right] \right\}, \quad S = \frac{4}{15} \pi^3 r_+^6, \quad (45)$$

where

$$\tilde{r}_+ = r_+ l^{-1}, \quad \tilde{q} = ql^{-4.5}, \quad \tilde{A}'_i(r_+) = l^{0.5} A'_i(r_+), \quad \tilde{h} = hl^{-1.5}, \quad \tilde{T} = Tl. \quad (46)$$

Moreover, the rescaled Gibbs free energy is given by

$$\tilde{F} \equiv F/l^5 = \tilde{F}(\tilde{T}, \tilde{q}, \tilde{h}). \quad (47)$$

By solving Eq. (40), we can obtain

$$\tilde{A}'_{ii}(r_+) = \frac{2\tilde{h}}{\sqrt{3}\tilde{r}_+^2} \cos \left[\frac{1}{3} \arccos \left(\frac{3\sqrt{3}\tilde{q}}{2\tilde{h}^3} \right) - \frac{2\pi}{3} (i-1) \right], \quad i = 1, 2, 3. \quad (48)$$

To clearly present the existence domain and the relative magnitude of three solutions, we define

$$C_i(x) \equiv \cos \left[\frac{1}{3} \arccos(x) - \frac{2\pi}{3} (i-1) \right] \quad (i = 1, 2, 3), \quad (49)$$

which is independent of \tilde{r}_+ . Then, three solutions can be expressed as

$$\tilde{A}'_{ii}(\tilde{r}_+) = \frac{2\tilde{h}}{\sqrt{3}\tilde{r}_+^2} C_i(x), \quad i = 1, 2, 3, \quad (50)$$

where $x = 3\sqrt{3}\tilde{q}/2\tilde{h}^3$. We display $C_i(x)$ in the left panel of Fig. 2(a). It is shown that there is no solution for $\tilde{A}'_{i2}(r_+)$ and $\tilde{A}'_{i3}(r_+)$ when $3\sqrt{3}\tilde{q}/2\tilde{h}^3 > 1$ and no solution for $\tilde{A}'_{i2}(r_+)$ and $\tilde{A}'_{i1}(r_+)$ when $3\sqrt{3}\tilde{q}/2\tilde{h}^3 < -1$. In the same manner, the Hawking temperature can be written as

$$\tilde{T}_i(\tilde{r}_+; \tilde{h}, x) = \frac{1}{4\pi\tilde{r}_+} \left\{ 5 + 7\tilde{r}_+^2 + \frac{\tilde{r}_+^2}{6} \left[\left(\frac{2\tilde{h}^2}{3\tilde{r}_+^4} C_i^2(x) - \frac{\tilde{h}^2}{2\tilde{r}_+^4} \right)^2 - \frac{2\tilde{h}\tilde{q}}{\sqrt{3}\tilde{r}_+^8} C_i(x) \right] \right\} \quad (51)$$

$$= \frac{1}{4\pi\tilde{r}_+} \left[5 + 7\tilde{r}_+^2 + \frac{\tilde{h}^4}{6\tilde{r}_+^6} D_i(x) \right], \quad (52)$$

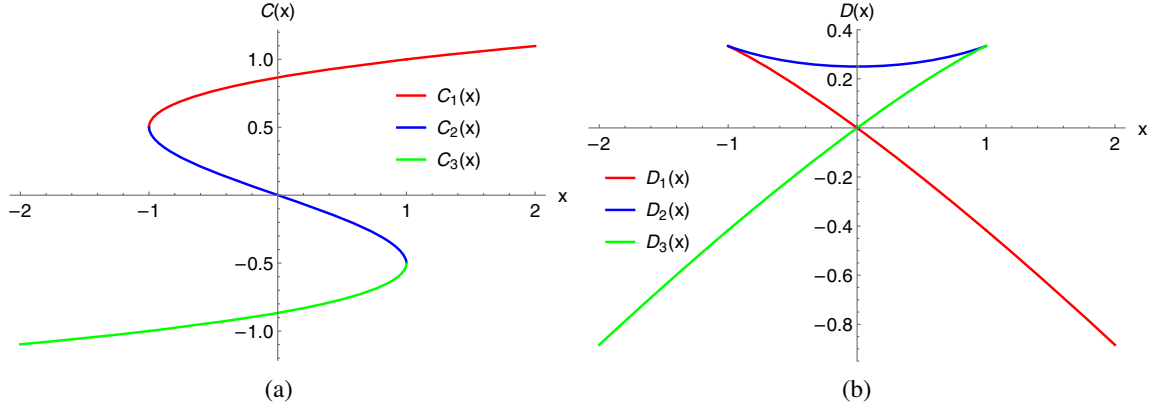


FIG. 2. $C(x)$ and $D(x)$, where $x \equiv \frac{3\sqrt{3}\tilde{q}}{2\tilde{h}^3}$. (a) $C(x)$. (b) $D(x)$.

and here

$$D_i(\tilde{h}, \tilde{q}) \equiv \frac{1}{4} \left[\frac{4C_i^2(\tilde{h}, \tilde{q})}{3} - 1 \right]^2 - C_i(\tilde{h}, \tilde{q}) \frac{2\tilde{q}}{\sqrt{3}\tilde{h}^3}, \quad (53)$$

which is shown in the right panel of Fig. 2(b). Equation (52) shows that $\tilde{h}^4 D_i(x)$ completely determines the dependence of $\tilde{T}_i(\tilde{r}_+)$ on \tilde{r}_+ . And because of the symmetry for $D_i(x)$, we only need to consider the case of $\tilde{h}\tilde{q} > 0$, i.e., $x > 0$. Moreover, note that three curves of $D_i(x)$ never intersect when $x > 0$, which means that $\tilde{T}_2(\tilde{r}_+) > \tilde{T}_3(\tilde{r}_+) > \tilde{T}_1(\tilde{r}_+)$ is always satisfied for fixed \tilde{h} and \tilde{q} and $\tilde{h}\tilde{q} > 0$. Moreover, the rescaled Gibbs free energy is

$$\tilde{F}_i = \frac{12\pi^2 \tilde{r}_+^5}{5} + \frac{16\pi^2 \tilde{r}_+^7}{5} - \frac{28}{15} \pi^3 \tilde{r}_+^6 \tilde{T}_i, \quad i = 1, 2, 3. \quad (54)$$

To find the critical point, one usually consider the equations

$$\frac{\partial \tilde{T}(\tilde{r})}{\partial \tilde{r}_+} = 0 \quad \text{and} \quad \frac{\partial^2 \tilde{T}(\tilde{r}_+)}{\partial \tilde{r}_+^2} = 0, \quad (55)$$

which can be solved as

$$\tilde{r}_{+c} = \sqrt{\frac{15}{28}}, \quad \tilde{T}_c = \sqrt{\frac{60}{7\pi^2}} \quad \text{and} \quad \tilde{h}^4 D_1(x) = -2 \left(\frac{15}{28} \right)^4. \quad (56)$$

As shown in the right panel of Fig. 2(b), $D_2(\tilde{h}, \tilde{q})$ and $D_3(\tilde{h}, \tilde{q})$ are always positive when $\tilde{h}\tilde{q} > 0$, which means that there is no critical point for \tilde{T}_2 and \tilde{T}_3 . And only $\tilde{T}(\tilde{r}_+)$ has a critical point. The detailed results about the existence of the local extremums are summarized in Table I.

As shown in Fig. 1(b), solving Eq. (52) for \tilde{r}_+ in terms of \tilde{T} gives $\tilde{r}_+(\tilde{T})$, which is usually a multivalued function. The parameters \tilde{h} and \tilde{q} determine the number of the branches for $\tilde{r}_+(\tilde{T})$. In what follows, we can find four major regions in the \tilde{h} - \tilde{q} plane if we only consider the number of branches of $\tilde{r}_+(\tilde{T})$. We plot these regions in the \tilde{h} - \tilde{q} plane, which is shown in Fig. 3. The left panel displays four major regions, and the right panel highlights region I and shows us five subregions of region I. Each region has the distinct behavior of the branches and the phase structure. In Fig. 4, we display the plots of event horizon \tilde{r}_+ , free energy \tilde{F} against the temperature \tilde{T} for Region I, while the ones for other regions (II, IV, and V) are shown in Fig. 5. The first-order phase transition and zeroth-order phase transition are marked with a black point and arrow, respectively.

(i) *Region I.*— $x < 1$ and $\tilde{T}'_1(\tilde{r}_1) < 0$, where \tilde{r}_1 is the solution of $\tilde{T}''_1(\tilde{r}_+) = 0$.

In this region, there are a local maximum and a local minimum for $\tilde{T}_1(\tilde{r}_+)$. Therefore, there are three branches for $\tilde{r}_{+1}(\tilde{T})$: the smallest BH for $0 \leq \tilde{T}_1 \leq \tilde{T}_{1\max}$, intermediate BH for $\tilde{T}_{1\min} \leq \tilde{T}_1 \leq \tilde{T}_{1\max}$, and largest BH for $\tilde{T}_1 \geq \tilde{T}_{1\min}$. However, there

TABLE I. Solution of $\tilde{T}'_i(\tilde{r}_+) = 0$ and the local extremums of $\tilde{T}'_i(\tilde{r}_+)$ in various cases, where \tilde{r}_1 is the solution of $\tilde{T}''_i(\tilde{r}_+) = 0$.

$\tilde{h}\tilde{q} > 0$, i.e., $x > 0$	$\tilde{T}'(0)$	$\tilde{T}'(+\infty)$	Solution of $\tilde{T}''(\tilde{r}_+) = 0$	Extrema of $\tilde{T}'(\tilde{r}_+)$
$T_1, \tilde{h}^4 D_1(x) > -2\left(\frac{15}{28}\right)^4$	∞	$\frac{7}{4\pi}$	$\tilde{r}_1 > 0$	$\tilde{T}'_{\min}(\tilde{r}_1) < 0$
$T_1, \tilde{h}^4 D_1(x) < -2\left(\frac{15}{28}\right)^4$	∞	$\frac{7}{4\pi}$	$\tilde{r}_1 > 0$	$\tilde{T}'_{\min}(\tilde{r}_1) > 0$
T_2 , exists for $x < 1$	$-\infty$	$\frac{7}{4\pi}$	None	None
T_3 , exists for $x < 1$	$-\infty$	$\frac{7}{4\pi}$	None	None

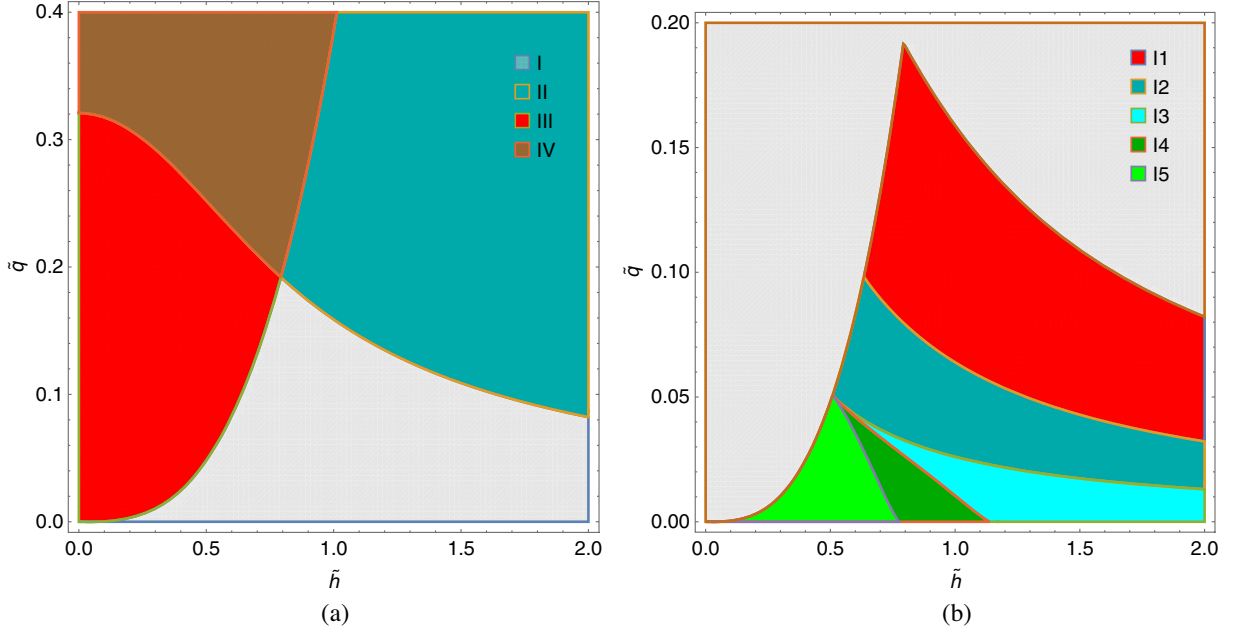


FIG. 3. The eight regions in the \tilde{h} - \tilde{q} plane for dyonic PM AdS black holes. The color represents the branch which enters at first phase transition with increasing \tilde{T} from 0 (except region IV), the darker color represents the zeroth-order phase transition, and the lighter color represents the first-order phase transition. (a) The four main regions in the \tilde{h} - \tilde{q} plane, each of which possesses the distinct behavior of the branches and the phase structure. (b) The five subregions of region I in the \tilde{h} - \tilde{q} plane, each of which possesses the distinct phase structure.

are a minimum $\tilde{T}_{2\min}$ for $\tilde{T}_2(\tilde{r}_+)$ and a minimum $\tilde{T}_{3\min}$ for $\tilde{T}_3(\tilde{r}_+)$, and thus two branches exist for $\tilde{r}_{+2}(\tilde{T})$ or $\tilde{r}_{+3}(\tilde{T})$, namely, a small BH and large BH for $\tilde{r}_{+2}(\tilde{T})$, smaller BH and larger BH for $\tilde{r}_{+3}(\tilde{T})$. The $\tilde{r}_+(\tilde{T})$ is displayed in the left panel of Fig. 4(a), and the Gibbs free energy is plotted in the following five panels for different subregions, which show different phase transitions. Note that the smallest BH, large BH, larger BH, and largest BH branches have positive heat capacity, and hence they are thermally stable (represented by solid lines), while others are thermally unstable (represented by dashed lines). First, the three tips in five figures of $\tilde{F}(\tilde{T})$ correspond to three minima of \tilde{T} with $\tilde{T}_{1\min} < \tilde{T}_{3\min} < \tilde{T}_{2\min}$ and $\tilde{F}_1(\tilde{T}_{1\min}) > \tilde{F}_3(\tilde{T}_{3\min}) > \tilde{F}_2(\tilde{T}_{2\min})$. And the $\tilde{F}(\tilde{T})$ of the smallest BH can intersect with that of other three stable phases with some parameter configuration [such as in Fig. 4(f)]. Three intersections $\tilde{T}_{1p} > \tilde{T}_{3p} > \tilde{T}_{2p}$ correspond to the largest BH (red), larger BH (light blue), and large BH (green). The difference of phase transitions is determined by the relative position of three minima and three intersections in the $\tilde{T} - \tilde{F}$ plane.

In subregion II as shown in Fig. 4(b), a first-order phase transition from smallest BH to largest BH occurs at $\tilde{T} = \tilde{T}_{1p}$ as \tilde{T} increases from 0, and then there are zeroth-order phase transitions at $\tilde{T} = \tilde{T}_{3\min}$ and $\tilde{T}_{2\min}$. (When $x = 1$, it is similar except \tilde{T}_2 and \tilde{T}_3 merge into one.)

In Fig. 4(c), we present the case of subregion I2, which is similar to the case of subregion II, where \tilde{T}_{2p} and \tilde{T}_{3p} do not exist since $\tilde{F}_2(\tilde{T})$ and $\tilde{F}_3(\tilde{T})$ are always smaller than \tilde{F} of the smallest BH, and $\tilde{T}_{1p} > \tilde{T}_{3\min}$. These results in two zeroth-order phase transitions occur at $\tilde{T} = \tilde{T}_{3\min}$ and $\tilde{T}_{2\min}$.

Figure 4(d) shows us the case of subregion I3, where \tilde{T}_{2p} still does not exist, however $\tilde{T}_{3p} < \tilde{T}_{2\min}$. Therefore, as one increases \tilde{T} from 0, there are a first-order phase transition at $\tilde{T} = \tilde{T}_{3p}$ and a zeroth-order phase transition at $\tilde{T} = \tilde{T}_{2\min}$.

In subregion I4, as shown in Fig. 4(e), \tilde{T}_{2p} does not exist since $\tilde{F}_2(\tilde{T})$ is always smaller than the free energy of the smallest BH, and $\tilde{T}_{2\min} < \tilde{T}_{3p} < \tilde{T}_{1p}$, which means that a zeroth-order phase transition between smallest BH and large BH happens at $\tilde{T} = \tilde{T}_{2\min}$ as \tilde{T} increases from 0.

The case of subregion I5 is displayed in Fig. 4(f), where all three intersections exist with $\tilde{T}_{2p} < \tilde{T}_{3p} < \tilde{T}_{1p}$. Therefore, only a first-order phase transition happens between smallest BH and large BH at $\tilde{T} = \tilde{T}_{2p}$. There is no phase transition when $\tilde{T} > \tilde{T}_{2p}$ since it is shown that $\tilde{F}_1(\tilde{T}) > \tilde{F}_3(\tilde{T}) > \tilde{F}_2(\tilde{T})$ for the largest BH, larger BH, and large BH.

- (ii) *Region II.*— $x < 1$ and $\tilde{T}'_1(\tilde{r}_1) \geq 0$. In this region, $\tilde{T}_1(\tilde{r}_+)$ is a monotonically increasing function, and there is only one largest BH branch for $\tilde{r}_{+1}(\tilde{T})$, which

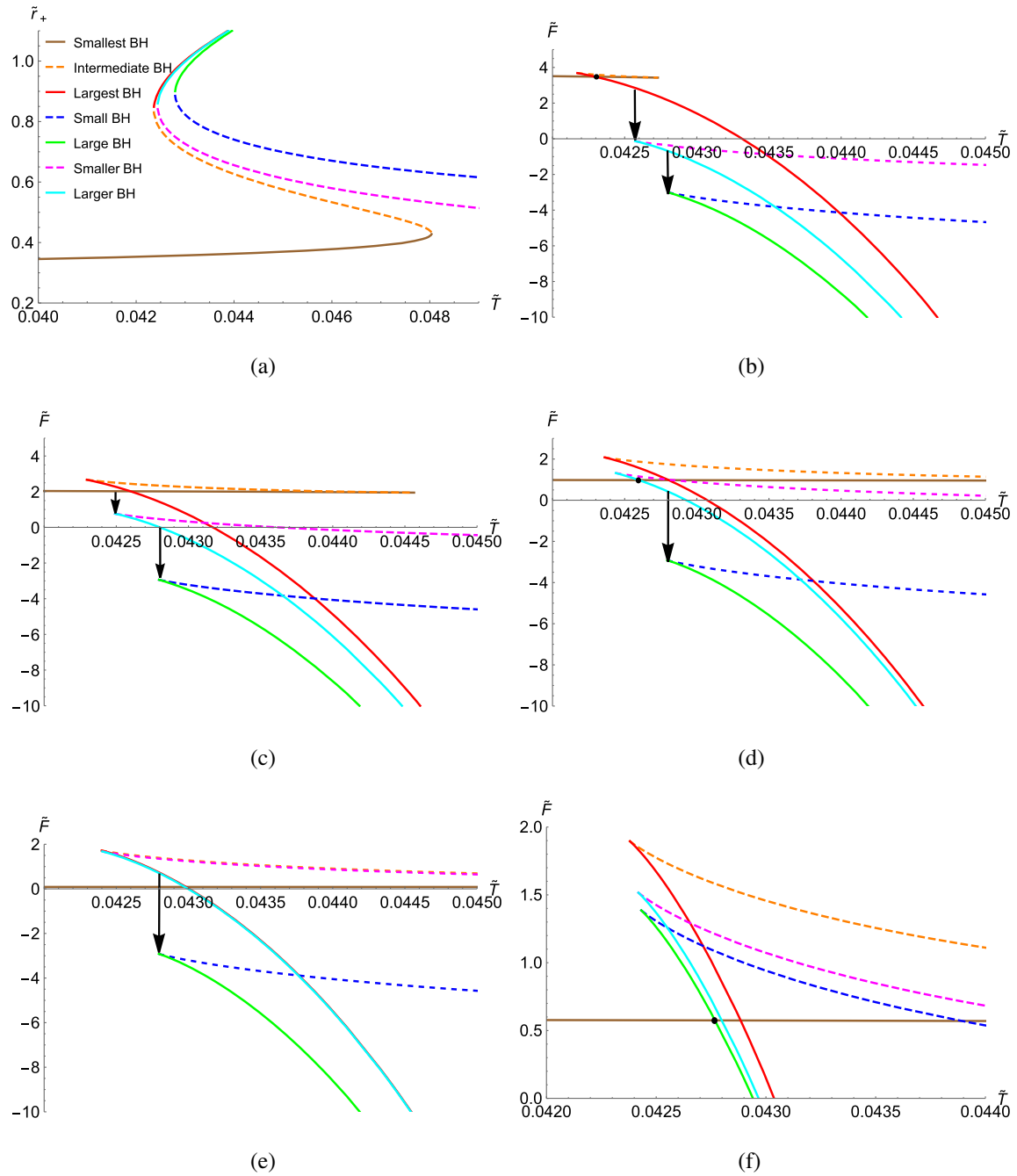


FIG. 4. \tilde{r}_+ , \tilde{F} against \tilde{T} for dyonic PM AdS black holes in region I. (a) Region I: $\tilde{h} = 1$ and $\tilde{q} = 0.02$. (b) Region II: $\tilde{h} = 1$ and $\tilde{q} = 0.1$. (c) Region I2: $\tilde{h} = 1$ and $\tilde{q} = 0.05$. (d) Region I3: $\tilde{h} = 1$ and $\tilde{q} = 0.02$. (e) Region I4: $\tilde{h} = 1$ and $\tilde{q} = 0.001$. (f) Region I5: $\tilde{h} = 0.5$ and $\tilde{q} = 0.02$.

is thermally stable. And there are still a minimum $\tilde{T}_{2\min}$ for $\tilde{T}_2(\tilde{r}_+)$ and a minimum $\tilde{T}_{3\min}$ for $\tilde{T}_3(\tilde{r}_+)$ indicating that $\tilde{r}_{+2}(\tilde{T})$ and $\tilde{r}_{+3}(\tilde{T})$ have two branches, which is the same as the case of region I. These features are displayed in Fig. 5(a), in which the left panel is $\tilde{r}_+(\tilde{T})$ and the free energy is plotted in the right panel. The large BH, larger BH, and largest BH branches are thermally stable. Since $\tilde{F}_1(\tilde{T}) > \tilde{F}_3(\tilde{T}) > \tilde{F}_2(\tilde{T})$ is always satisfied, there are a zeroth-order phase

transition from largest BH to larger BH at $\tilde{T} = \tilde{T}_{3\min}$ and a zeroth-order phase transition from larger BH to large BH at $\tilde{T} = \tilde{T}_{2\min}$. (If $x = 1$, it is similar, except \tilde{T}_2 and \tilde{T}_3 merge into one.)

- (iii) *Region III.*— $x > 1$ and $\tilde{T}'_1(\tilde{r}_1) < 0$. In this region, there are a local maximum and a local minimum for $\tilde{T}_1(\tilde{r}_+)$, similar to the case of region I. However, \tilde{T}_2 and \tilde{T}_3 do not exist, so there is only one first-order phase transition from the smallest BH to largest BH

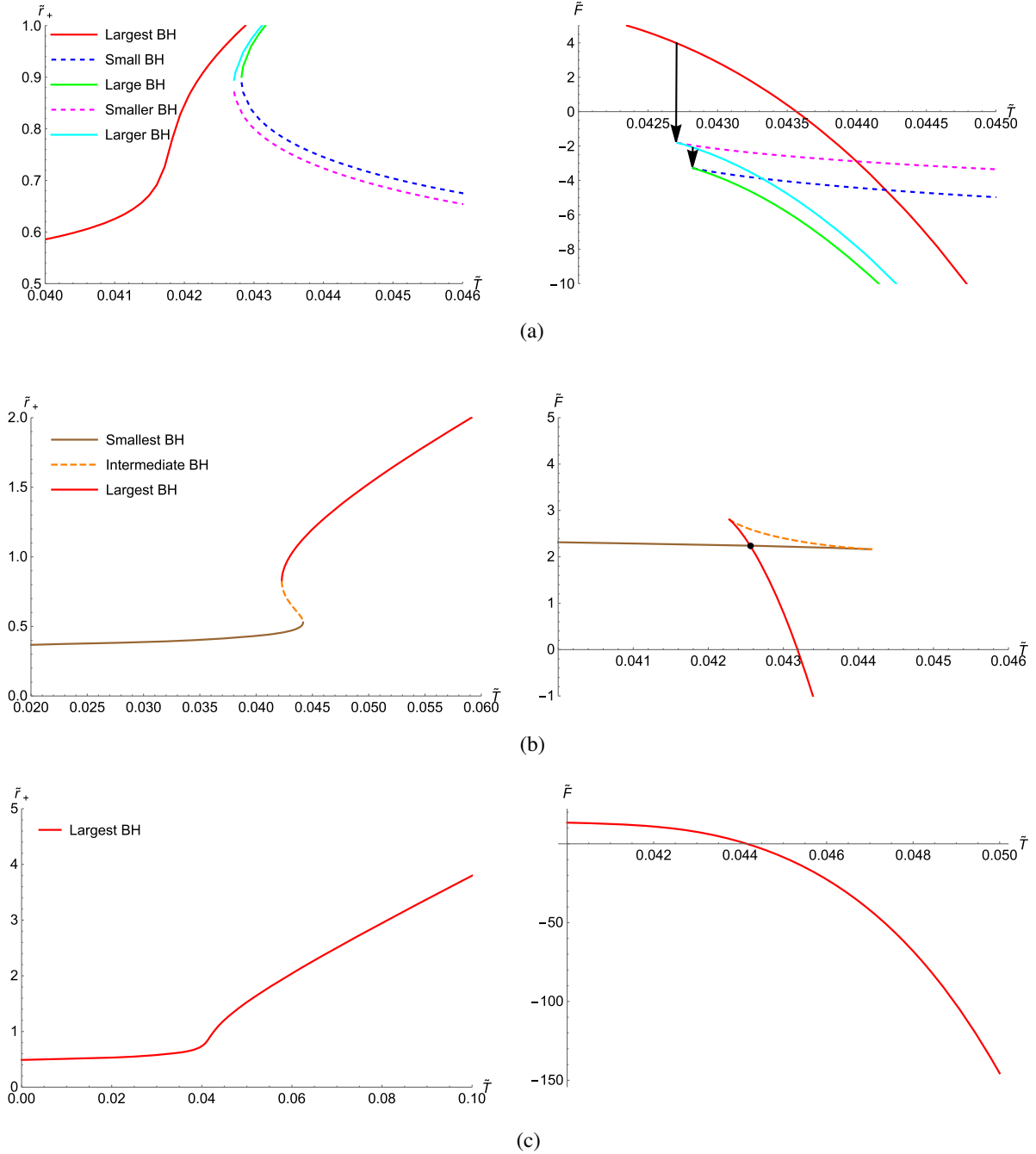


FIG. 5. \tilde{r}_+ , \tilde{F} against \tilde{T} for dyonic PM AdS black holes in regions II, III, and IV. The number of branches is different in these regions. The intermediate BH, small BH, and smaller BH are always thermally unstable, while others are always thermally stable. (a) Region II: $\tilde{h} = 1$ and $\tilde{q} = 0.2$. There is a zeroth-order phase transition between largest BH and larger BH and a zeroth-order phase transition between larger BH and large BH. (b) Region III: $\tilde{h} = 0.5$ and $\tilde{q} = 0.1$. There is a first-order phase transition between smallest BH and largest BH. (c) Region IV: $\tilde{h} = 0.5$ and $\tilde{q} = 0.3$. There is no phase transition.

at $\tilde{T} = \tilde{T}_{1p}$, which resembles that of RN-AdS black holes. These are displayed in the left panel of Fig. 5(b). The smallest BH and largest BH branches are thermally stable, while the intermediate BH is unstable.

(iv) *Region IV.*— $x > 1$ and $\tilde{T}'_1(\tilde{r}_1) \geq 0$. In this region, $\tilde{T}_1(\tilde{r}_+)$ is a monotonically increasing function and

has only one branch. Moreover, \tilde{T}_2 and \tilde{T}_3 do not exist, so there is no phase transition in this region, which is displayed in Fig. 5(c).

We now discuss the critical behavior and phase structure of black holes in two aspects. The critical line is the boundary between the two regions in which $\tilde{T}(\tilde{r}_+)$ has n and $n + 2$ extremums, determined by Eq. (55). In our case,

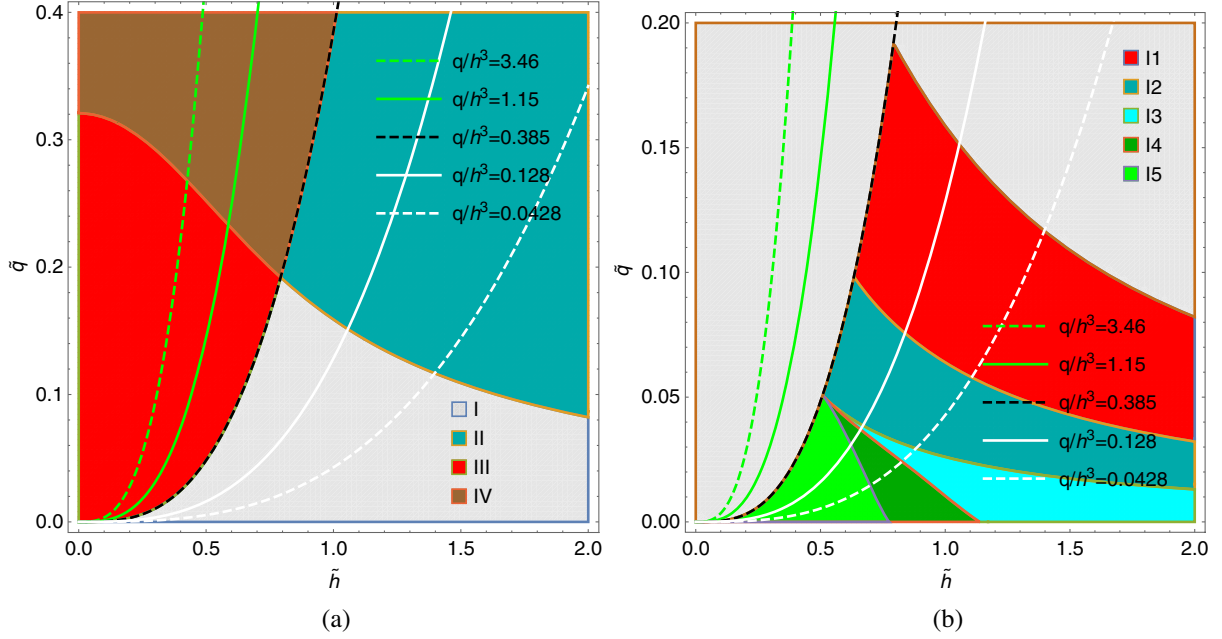


FIG. 6. In the case of varying AdS radius l (the pressure P) with fixed q and h , the system moves along $\tilde{q}_l(\tilde{h})$, which is displayed for various values of q/h^3 . There is always a critical point and a corresponding largest BH/smallest BH first-order phase transition.

the critical line is the boundary between the two regions in which $\tilde{T}(\tilde{r}_+)$ has no extremum and 2 extremums, i.e., the boundary of region I and region II or the boundary of region III and region IV.

On the one hand, we fix parameters q and h , and the AdS radius l (the pressure P) varies. This would generate a curve in the \tilde{h} - \tilde{q} plane, which is determined by

$$\tilde{q}_l(\tilde{h}) = \frac{q}{h^3} \tilde{h}^3. \quad (57)$$

In Fig. 6, we plot $\tilde{q}_l(\tilde{h})$ for various values of q/h^3 . It shows that there is always a critical point as P increases from 0 to ∞ since the critical line can extend to $\tilde{h} = +\infty$. For $q/h^3 > 2\sqrt{3}/9$, as one increases P from 0, $\tilde{q}_l(\tilde{h})$ always crosses the critical line and enters region IV (no phase transition) from region III (a first-order phase transition between the smallest BH and largest BH). For $q/h^3 < 2\sqrt{3}/9$, as one increases P from 0, $\tilde{q}_l(\tilde{h})$ passes through five subregions of region I, then crosses the critical line and enters region II, in which there are two zeroth-order phase transitions, one from the largest BH to the larger BH and one from the larger BH to the large BH.

On the other hand, h and P are fixed parameters. As one increases \tilde{q} from $\tilde{q} = 0$, the black hole would cross different regions. And there is always a critical point for any \tilde{h} since the critical line can extend to $\tilde{h} = +\infty$. In Fig. 7, we present phase diagrams in the $\tilde{q} - \tilde{T}$ plane with $\tilde{h} = 0.5$, $\tilde{h} = 0.6$, $\tilde{h} = 0.7$, and $\tilde{h} = 1$, respectively. The phase structure can be manifested more clearly in these phase diagrams, where the blue lines (point) represent

first-order phase transitions, the red lines (point) represent zeroth-order phase transitions, and the black points represent the critical points.

For $\tilde{h} \leq \tilde{h}_1 \simeq 0.51$, as one increases \tilde{q} from $\tilde{q} = 0$, the black hole would cross three regions subsequently, i.e., region I5 (smallest BH/large BH first-order phase transition) \rightarrow region III (the smallest BH/largest BH first-order phase transition) \rightarrow region IV (no phase transition), as shown in Fig. 7(a).

For $\tilde{h}_1 \leq \tilde{h} < \tilde{h}_2 \simeq 0.63$, the black hole will cross three more regions, i.e., region I5 (smallest BH/large BH first-order phase transition) \rightarrow region I4 (smallest BH/large BH zeroth-order phase transition) \rightarrow region I3 (a smallest BH/larger BH first-order phase transition and a larger BH/large BH zeroth-order phase transition) \rightarrow region I2 (a smallest BH/larger BH zeroth-order phase transition and a larger BH/large BH zeroth-order phase transition) \rightarrow region III (the smallest BH/largest BH first-order phase transition) \rightarrow region IV (no phase transition). These are shown in Fig. 7(b).

When $\tilde{h}_2 \leq \tilde{h} < \tilde{h}_3 \simeq 0.76$, the process becomes region I5 (smallest BH/large BH first-order phase transition) \rightarrow region I4 (smallest BH/large BH zeroth-order phase transition) \rightarrow region I3 (a smallest BH/larger BH first-order phase transition and a larger BH/large BH zeroth-order phase transition) \rightarrow region I2 (a smallest BH/larger BH zeroth-order phase transition and a larger BH/large BH zeroth-order phase transition) \rightarrow region I1 (the smallest BH/largest BH first-order phase transition and two zeroth-order phase transitions) \rightarrow region III (the smallest BH/largest BH first-order phase transition) \rightarrow region IV (no phase transition), which is shown in Fig. 7(c).

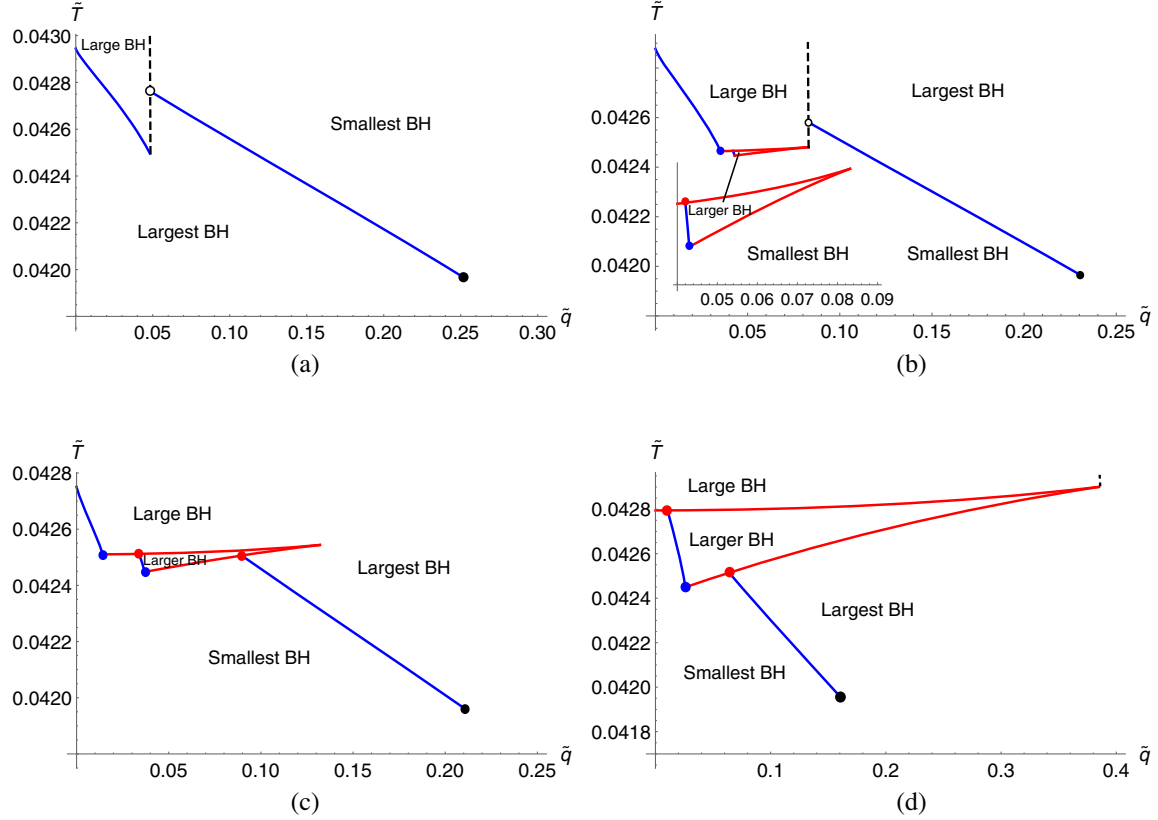


FIG. 7. The phase diagram in the \tilde{q} - \tilde{T} plane for dyonic PM AdS black holes with $\tilde{h} = 0.5$, $\tilde{h} = 0.6$, $\tilde{h} = 0.7$, and $\tilde{h} = 1$. The blue line and point represents first-order phase transition, and the red line and point represents zeroth-order transition. The black point represents the critical point. (a) $\tilde{h} = 0.5$. (b) $\tilde{h} = 0.6$. (c) $\tilde{h} = 0.7$. (d) $\tilde{h} = 1$.

When $\tilde{h} \geq \tilde{h}_3 \simeq 0.76$, it becomes region I4 (smallest BH/large BH zeroth-order phase transition) \rightarrow region I3 (a smallest BH/larger BH first-order phase transition and a larger BH/large BH zeroth-order phase transition) \rightarrow region I2 (a smallest BH/larger BH zeroth-order phase transition and a larger BH/large BH zeroth-order phase transition) \rightarrow region II (the smallest BH/largest BH first-order phase transition and two zeroth-order phase transitions) \rightarrow region III (the smallest BH/largest BH first-order phase transition) \rightarrow region IV (no phase transition), as shown in Fig. 7(d).

When $\tilde{h} \geq \tilde{h}_4 \simeq 1.14$, it just begins from region I3; therefore, it is comparable to Fig. 7(d), except that the red line before the blue line on the left is cut.

IV. CONCLUSION

We have investigated the thermodynamic behavior of d -dimensional dyonic PM AdS black holes in the extended phase space, which includes the conjugate pressure/volume quantities. The black hole temperature T , charge q , horizon radius r_+ (thermodynamic volume V), AdS radius l (pressure P), and the magnetic parameter h could be connected by

$$Tl = \tilde{T}(r_+/l, q/l^a, h/l^b), \quad (58)$$

where a and b depend on the dimension d and the power exponent p . In the canonical ensemble with fixed T and q , we found that the critical behavior and phase structure of the black hole are determined by $\tilde{q} \equiv q/l^a$ and $\tilde{h} \equiv h/l^b$.

For eight-dimensional dyonic PM AdS black holes with a power exponent 2, we identified different parameter configurations according to their characteristic phase transitions in the $\tilde{h} - \tilde{q}$ plane, which is shown in Fig. 3. There are eight regions, and each region has a different phase behavior. Then, we studied the phase transition with fixed $\tilde{q} \equiv q/l^a$ and $\tilde{h} \equiv h/l^b$ in Figs. 4 and 5, in which the thermal stabilities of the black holes have been examined and it was found that all the thermodynamically preferred phases are thermally stable. Furthermore, in Fig. 6, the variation of P was also investigated in the $\tilde{h} - \tilde{q}$ plane. There is always a critical point as P increases from 0 to ∞ since the critical line can extend to $\tilde{h} = +\infty$. Finally, we displayed the phase structure of the black hole in the $\tilde{h} - \tilde{T}$ plane with different \tilde{q} , as plotted in Fig. 7. Unlike RN-AdS black holes, the temperature $\tilde{T}(\tilde{r}_+, \tilde{q}, \tilde{h})$ of dyonic PM AdS black holes could have more than one branch for some parameter configurations of \tilde{q} and \tilde{h} . If we discuss them

separately, one of them (\tilde{T}_1) resembles the temperature of RN-AdS black holes, and the other two (if they exist) resemble that of Schwarzschild-AdS black holes. This feature results in complex phase structures and phase behaviors.

ACKNOWLEDGMENTS

We are grateful to Peng Wang, Yuchen Huang, Ningchen Bai, and Jiayi Wu for useful discussions. This work is supported by NSFC (Grant No. 12147207).

-
- [1] Werner Israel, Event horizons in static vacuum space-times, *Phys. Rev.* **164**, 1776 (1967).
 - [2] S. W. Hawking, Gravitational Radiation from Colliding Black Holes, *Phys. Rev. Lett.* **26**, 1344 (1971).
 - [3] Jacob D Bekenstein, Black holes and the second law, *Lett. Nuovo Cimento* **4**, 737 (1972).
 - [4] Jacob D. Bekenstein, Black holes and entropy, *Phys. Rev. D* **7**, 2333 (1973).
 - [5] James M. Bardeen, B. Carter, and S. W. Hawking, The four laws of black hole mechanics, *Commun. Math. Phys.* **31**, 161 (1973).
 - [6] S. W. Hawking, Particle creation by black holes, *Commun. Math. Phys.* **43**, 199 (1975); **46**, 206(E) (1976).
 - [7] S. W. Hawking and Don N. Page, Thermodynamics of black holes in anti-De Sitter space, *Commun. Math. Phys.* **87**, 577 (1983).
 - [8] G. W. Gibbons and S. W. Hawking, Cosmological event horizons, thermodynamics, and particle creation, *Phys. Rev. D* **15**, 2738 (1977).
 - [9] Juan Martin Maldacena, The large N limit of superconformal field theories and supergravity, *Int. J. Theor. Phys.* **38**, 1113 (1999).
 - [10] Edward Witten, Anti-de Sitter space, thermal phase transition, and confinement in gauge theories, *Adv. Theor. Math. Phys.* **2**, 505 (1998).
 - [11] Andrew Chamblin, Roberto Emparan, Clifford V. Johnson, and Robert C. Myers, Charged AdS black holes and catastrophic holography, *Phys. Rev. D* **60**, 064018 (1999).
 - [12] Andrew Chamblin, Roberto Emparan, Clifford V. Johnson, and Robert C. Myers, Holography, thermodynamics and fluctuations of charged AdS black holes, *Phys. Rev. D* **60**, 104026 (1999).
 - [13] Brian P. Dolan, Pressure and volume in the first law of black hole thermodynamics, *Classical Quantum Gravity* **28**, 235017 (2011).
 - [14] David Kubiznak and Robert B. Mann, P-V criticality of charged AdS black holes, *J. High Energy Phys.* **07** (2012) 033.
 - [15] David Kastor, Sourya Ray, and Jennie Traschen, Enthalpy and the mechanics of AdS black holes, *Classical Quantum Gravity* **26**, 195011 (2009).
 - [16] Shao-Wen Wei and Yu-Xiao Liu, Critical phenomena and thermodynamic geometry of charged Gauss-Bonnet AdS black holes, *Phys. Rev. D* **87**, 044014 (2013).
 - [17] Rong-Gen Cai, Li-Ming Cao, Li Li, and Run-Qiu Yang, P-V criticality in the extended phase space of Gauss-Bonnet black holes in AdS space, *J. High Energy Phys.* **09** (2013) 005.
 - [18] Wei Xu and Liu Zhao, Critical phenomena of static charged AdS black holes in conformal gravity, *Phys. Lett. B* **736**, 214 (2014).
 - [19] Antonia M. Frassino, David Kubiznak, Robert B. Mann, and Fil Simovic, Multiple reentrant phase transitions and triple points in Lovelock thermodynamics, *J. High Energy Phys.* **09** (2014) 080.
 - [20] M. H. Dehghani, S. Kamrani, and A. Sheykhi, $P - V$ criticality of charged dilatonic black holes, *Phys. Rev. D* **90**, 104020 (2014).
 - [21] Robie A. Hennigar, Wilson G. Brenna, and Robert B. Mann, $P - v$ criticality in quasitopological gravity, *J. High Energy Phys.* **07** (2015) 077.
 - [22] Olivera Miskovic and Rodrigo Olea, Quantum statistical relation for black holes in nonlinear electrodynamics coupled to Einstein-Gauss-Bonnet AdS gravity, *Phys. Rev. D* **83**, 064017 (2011).
 - [23] Olivera Miskovic and Rodrigo Olea, Conserved charges for black holes in Einstein-Gauss-Bonnet gravity coupled to nonlinear electrodynamics in AdS space, *Phys. Rev. D* **83**, 024011 (2011).
 - [24] Harald H. Soleng, Charged black points in general relativity coupled to the logarithmic U(1) gauge theory, *Phys. Rev. D* **52**, 6178 (1995).
 - [25] Eloy Ayon-Beato and Alberto Garcia, Regular Black Hole in General Relativity Coupled to Nonlinear Electrodynamics, *Phys. Rev. Lett.* **80**, 5056 (1998).
 - [26] Hideki Maeda, Mokhtar Hassaine, and Cristian Martinez, Lovelock black holes with a nonlinear Maxwell field, *Phys. Rev. D* **79**, 044012 (2009).
 - [27] S. H. Hendi, B. Eslam Panah, S. Panahiyan, and A. Sheykhi, Dilatonic BTZ black holes with power-law field, *Phys. Lett. B* **767**, 214 (2017).
 - [28] Jun Tao, Peng Wang, and Haitang Yang, Testing holographic conjectures of complexity with Born-Infeld black holes, *Eur. Phys. J. C* **77**, 817 (2017).
 - [29] Xiaobo Guo, Peng Wang, and Haitang Yang, Membrane paradigm and holographic DC conductivity for nonlinear electrodynamics, *Phys. Rev. D* **98**, 026021 (2018).
 - [30] Benrong Mu, Peng Wang, and Haitang Yang, Holographic DC conductivity for a power-law Maxwell field, *Eur. Phys. J. C* **78**, 1005 (2018).
 - [31] Peng Wang, Houwen Wu, and Haitang Yang, Holographic DC conductivity for backreacted nonlinear electrodynamics with momentum dissipation, *Eur. Phys. J. C* **79**, 6 (2019).
 - [32] Peng Wang, Houwen Wu, and Haitang Yang, Thermodynamics and phase transitions of nonlinear electrodynamics

- black holes in an extended phase space, *J. Cosmol. Astropart. Phys.* **04** (2019) 052.
- [33] Tianhao Bai, Wei Hong, Benrong Mu, and Jun Tao, Weak cosmic censorship conjecture in the nonlinear electro-dynamics black hole under the charged scalar field, *Commun. Theor. Phys.* **72**, 015401 (2020).
- [34] Peng Wang, Houwen Wu, and Haitang Yang, Thermodynamics and weak cosmic censorship conjecture in nonlinear electro-dynamics black holes via charged particle absorption, [arXiv:1904.12365](https://arxiv.org/abs/1904.12365).
- [35] Qingyu Gan, Peng Wang, and Haitang Yang, Temperature dependence of in-plane resistivity and inverse hall angle in NLED holographic model, *Commun. Theor. Phys.* **71**, 577 (2019).
- [36] Peng Wang, Houwen Wu, and Haitang Yang, Thermodynamics and phase transition of a nonlinear electro-dynamics black hole in a cavity, *J. High Energy Phys.* **07** (2019) 002.
- [37] Sharmanthie Fernando and Don Krug, Charged black hole solutions in Einstein-Born-Infeld gravity with a cosmological constant, *Gen. Relativ. Gravit.* **35**, 129 (2003).
- [38] De-Cheng Zou, Shao-Jun Zhang, and Bin Wang, Critical behavior of Born-Infeld AdS black holes in the extended phase space thermodynamics, *Phys. Rev. D* **89**, 044002 (2014).
- [39] S. H. Hendi and M. H. Vahidinia, Extended phase space thermodynamics and P-V criticality of black holes with a nonlinear source, *Phys. Rev. D* **88**, 084045 (2013).
- [40] Jie-Xiong Mo, Gu-Qiang Li, and Xiao-Bao Xu, Effects of power-law Maxwell field on the critical phenomena of higher dimensional dilaton black holes, *Phys. Rev. D* **93**, 084041 (2016).
- [41] Pavan Kumar Yerra and Bhamidipati Chandrasekhar, Heat engines at criticality for nonlinearly charged black holes, *Mod. Phys. Lett. A* **34**, 1950216 (2019).
- [42] Cao H. Nam, Non-linear charged dS black hole and its thermodynamics and phase transitions, *Eur. Phys. J. C* **78**, 418 (2018).
- [43] Mokhtar Hassaine and Cristian Martinez, Higher-dimensional black holes with a conformally invariant Maxwell source, *Phys. Rev. D* **75**, 027502 (2007).
- [44] S. H. Hendi and H. R. Rastegar-Sedehi, Ricci flat rotating black branes with a conformally invariant Maxwell source, *Gen. Relativ. Gravit.* **41**, 1355 (2009).
- [45] S. H. Hendi, Topological black holes in Gauss-Bonnet gravity with conformally invariant Maxwell source, *Phys. Lett. B* **677**, 123 (2009).
- [46] Mokhtar Hassaine and Cristian Martinez, Higher-dimensional charged black holes solutions with a nonlinear electro-dynamics source, *Classical Quantum Gravity* **25**, 195023 (2008).
- [47] S. H. Hendi and B. Eslam Panah, Thermodynamics of rotating black branes in Gauss-Bonnet-nonlinear Maxwell gravity, *Phys. Lett. B* **684**, 77 (2010).
- [48] S. H. Hendi, Slowly rotating black holes in Einstein-Generalized Maxwell gravity, *Prog. Theor. Phys.* **124**, 493 (2010).
- [49] S. H. Hendi, Rotating black branes in the presence of nonlinear electromagnetic field, *Eur. Phys. J. C* **69**, 281 (2010).
- [50] S. H. Hendi, Rotating black string with nonlinear source, *Phys. Rev. D* **82**, 064040 (2010).
- [51] J. D. Bekenstein, Black holes with scalar charge, *Ann. Phys. (N.Y.)* **91**, 75 (1975).
- [52] Cristian Martinez and Jorge Zanelli, Conformally dressed black hole in $(2 + 1)$ -dimensions, *Phys. Rev. D* **54**, 3830 (1996).
- [53] Marc Henneaux, Cristian Martinez, Ricardo Troncoso, and Jorge Zanelli, Black holes and asymptotics of $2 + 1$ gravity coupled to a scalar field, *Phys. Rev. D* **65**, 104007 (2002).
- [54] Bernard J. Kelly, Wolfgang Tichy, Manuela Campanelli, and Bernard F. Whiting, Black hole puncture initial data with realistic gravitational wave content, *Phys. Rev. D* **76**, 024008 (2007).
- [55] Cristian Martinez, Juan Pablo Staforelli, and Ricardo Troncoso, Topological black holes dressed with a conformally coupled scalar field and electric charge, *Phys. Rev. D* **74**, 044028 (2006).
- [56] B. C. Xanthopoulos and T. E. Dialynas, Einstein gravity coupled to a massless conformal scalar field in arbitrary space-time dimensions, *J. Math. Phys. (N.Y.)* **33**, 1463 (1992).
- [57] C. Klimcik, Search for the conformal scalar hair at arbitrary D, *J. Math. Phys. (N.Y.)* **34**, 1914 (1993).
- [58] F. R. Tangherlini, Schwarzschild field in n dimensions and the dimensionality of space problem, *Nuovo Cimento* **27**, 636 (1963).
- [59] J. C. Fabris, Cosmological model from generalized Maxwell-Einstein system in higher dimensions, *Phys. Lett. B* **267**, 30 (1991).
- [60] K. A. Bronnikov and J. C. Fabris, Multidimensional Reissner-Nordstrom problem with a generalized Maxwell field, *Gravitation Cosmol.* **2**, 306 (1996), <https://inspirehep.net/literature/428897>.
- [61] J. Jing, Q. Pan, and S. Chen, Holographic superconductors with Power-Maxwell field, *J. High Energy Phys.* **11** (2011) 045.
- [62] K. A. Bronnikov, Dyonic configurations in nonlinear electro-dynamics coupled to general relativity, *Gravitation Cosmol.* **23**, 343 (2017).
- [63] D. A. Rasheed, Non-linear electro-dynamics: Zeroth and first laws of black hole mechanics, [arXiv:hep-th/9702087](https://arxiv.org/abs/hep-th/9702087).